ÉCOLE POLYTECHNIQUE
FÉDÉRALE DE LAUSANNE

MASTER THESIS

Extensive air shower Monte Carlo simulations for a wide field of view Cherenkov telescope

Author:
Cyril Martin ALISPACH

Director:
Prof. Aurelio BAY
Supervisor:
Prof. Andrii NERONOV

A thesis submitted in fulfillment of the requirements for the degree of Master of Science in Physics

in the

Laboratoire de Physique des Hautes Energies LPHE
Institut de Physique IPHYS

June 17, 2016

ÉCOLE POLYTECHNIQUE FÉDÉRALE DE LAUSANNE

Abstract

Faculté
Institut de Physique IPHYS

Master of Science in Physics

Extensive air shower Monte Carlo simulations for a wide field of view Cherenkov telescope

by Cyril Martin ALISPACH

The work presents the performance of a wide field of view Cherenkov telescope. The telescope optics is composed of POLAR camera modules of window time $\Delta t \simeq 100$ ns with 1 m^2 Fresnel lenses for the optics. This design of telescope is motivated by recent new neutrino signal in the energy band from 30 TeV to 10 PeV observed by IceCube neutrino telescope. Wide FoV Cherenkov telescopes with wide time window could be able to detect the companion gamma ray at 100 TeV to clarify their origins. It could as well observe τ neutrino extensive air showers bellow the horizon in the 100 TeV to 100 PeV energy band. The time of arrival of Cherenkov light is studied for various distances to the shower axis where one concluded that the time window of POLAR could record gamma ray events up too 500 m without large bias on energy estimation. The effective area of the telescope was computed with Monte Carlo simulation using CORSIKA 74100 from which a minimum detection energy was found to be at 100 GeV with good sensitivity at energies beyond 100 TeV. The study also considers observations of extensive air showers with a test setup at the roof of the Geneva Observatory. Operation of Cherenkov telescopes at this location has a specific of high background produced by city light.

Acknowledgements

I express my gratitude to my supervisor Prof. Andrii Neronov for following the course of this work with me during the semester. I am grateful for all the useful comments and discussion we had on this work as well for his availability. I thank Prof. Andrii Neronov for allowing me to learn and work on gamma ray astronomy. I would like to thank my director Prof. Aurelio Bay for is contribution and support to this work and for allowing me access to the great infrastructure at the LPHE. My last gratitudes go to my family and closed friends for their support during this work and my studies at EPFL.

Contents

List of Figures

Chapter 1

Introduction to cosmic rays and Cherenkov telescopes

1.1 Discovery of cosmic rays

Cosmic rays were discovered in 1912 by Victor Hess. He studied the levels of ionizing radiation in the atmosphere by sending his detection equipment with balloons. At that time scientists expected the levels of ionizing radiation to be lower than on the Earth's surface because they thought that the radiation was only coming from the ground. Hess measured a decrease of radiation until he reached 1 km but after that point he observed that the radiation level was growing considerably. He concluded that a form of radiation was coming from space. Until 1927, it was believed that cosmic rays are of electromagnetic origin hence are photons. From this year the results of Jacob Clay showed a variation of intensity in cosmic rays with the latitude thus it proved that cosmic rays must be mainly charged particles. Following that discovery a higher intensity of cosmic rays on the west than on the east was observed and proved that they are positively charged. Today we know that cosmic ray particles are composed of protons, alpha particles, nuclei and a minor quantity (about 1%) are electrons, positrons, antiproton and gamma rays.

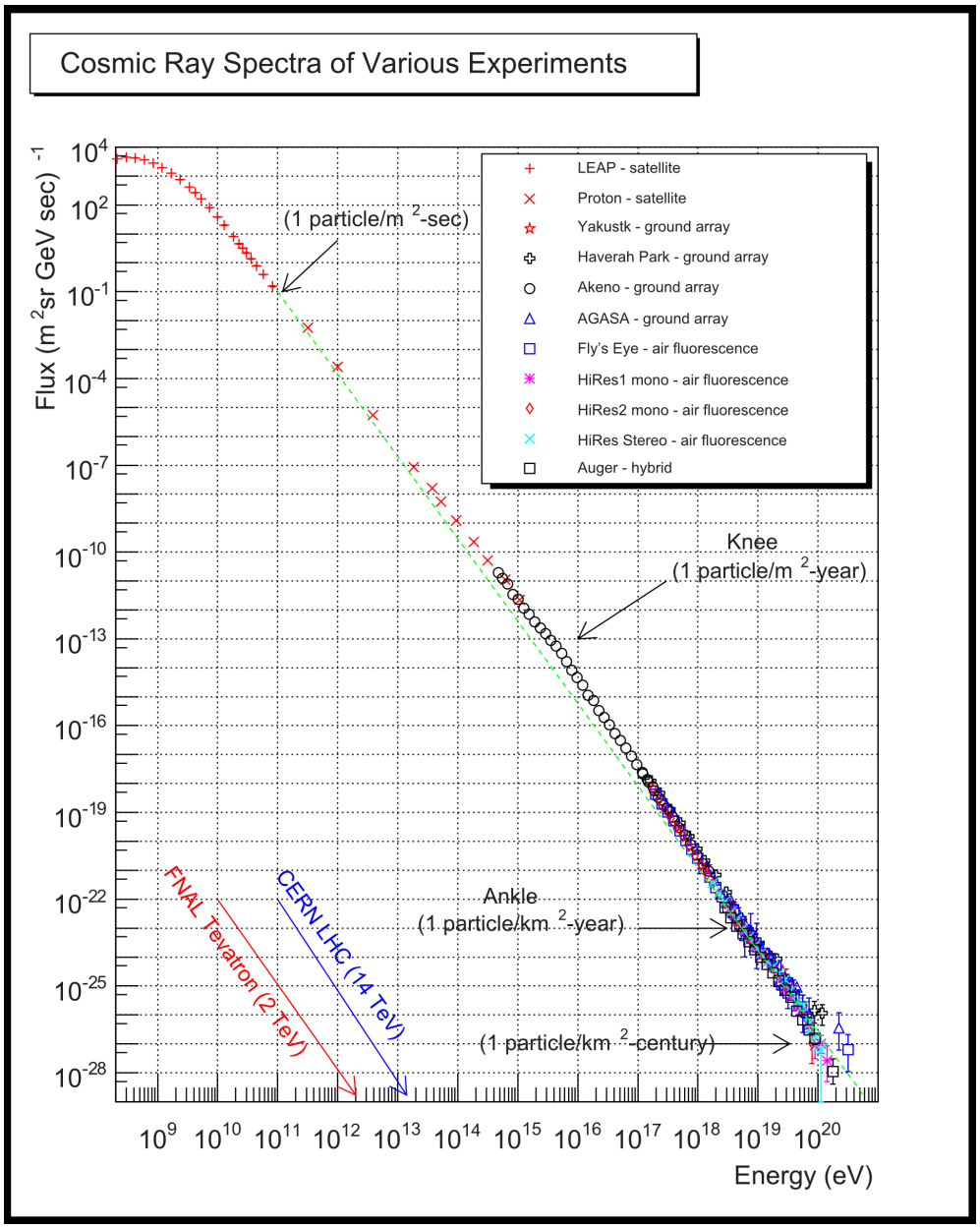

FIGURE 1.1: Cosmic ray spectrum from various experiments. Source: *What Are Cosmic Rays*

As shown on figure 1.1, cosmic rays energies are recorded up to 10^{20} eV and the flux diminishes rapidly with the energy. The flux is constant for energies from 10^{8} eV to 10^{9} eV which is explained by the fact that the particles are deflected by interplanetary and Earth's magnetic field and thus cannot be observed from the Earth. The upper limit in energy can be explained by the theoretical Greisen–Zatsepin–Kuzmin limit (GZK limit). It shows that for energies over 10^{20} eV protons would interact with CMB photons to produce pions via the Δ^{+} resonance $p + \gamma_{CMB} \rightarrow \Delta^{+} \rightarrow p, n + \pi^{0}, \pi^{+}$. The flux of cosmic rays can be expressed by a power law (Bay, 2014, 3, p. 28):

$$\frac{\mathrm{d}N}{\mathrm{d}E} \propto E^{-\alpha}, \tag{1.1}$$

where α varies within the energy regions as:

$$\alpha = \begin{cases} 2.7 & E < 10^{16}\ \text{eV} \\ 3.0 & 10^{16} < E < 10^{18}\ \text{eV} \\ 2.5 & E > 10^{18}\ \text{eV}. \end{cases} \tag{1.2}$$

The study of cosmic rays is of great importance in both astrophysics and particle physics. The Universe is a natural particle accelerator reaching energies much higher that the ones nowadays studied at CERN ($\simeq$ 14 TeV) and the Earth's atmosphere acts as a natural detector, making it an interesting field of study for particle physicists. Hess's discoveries in the beginning of the 20th century opened the doors to further progress in particle physics such as the discovery of the positron and the muon by Carl David Anderson in 1932 and 1936.

1.2 Origins of cosmic rays

The sources of cosmic rays are not well understood for now. However they could originate from active galactic nuclei, starburst galaxies, pulsars, pulsar wind nebulae and supernovae remnants of massive stars. This sources are of great interest for astrophysicist. It is also of great interest in the study of dark matter and Weakly Interacting Massive Particles (WIMPs) models.WIMPs could annihilate and produce quark-antiquark pairs and then would hit the Earth's atmosphere and produce showers that we observe. Cosmic ray flux could also have a contribution from interaction of dark matter particles. This hypothetical observations could then revolutionize and extend the standard model as the discovery of Hess led to the discovery of the positron and the muon. (*Comsic ray Wikipedia article*)

1.3 Context of study

Over the last decade major breakthroughs where done in gamma ray astronomy with Imaging Atmospheric Cherenkov Telecopes (IACTs). In the Very-High Energy band (VHE) HESS, MAGIC and VERITAS identified various new gamma ray sources. Next generation gamma ray observatory Cherenkov Telescope Array (CTA) is currently under development. It will observe on the VHE as well up to a 100 TeV. At this limit a collection area of about 10 km^2 and a larger than 10° field of view is needed . Arrays of Cherenkov telescopes of FoV between 30° and 60° would improve sensitivity at 100 TeV energies.

A recent new neutrino signal in the energy band from 30 TeV to 10 PeV has been observed by IceCube neutrino telescope. VHE neutrino production always comes with gamma ray. The source of these events is at the moment not established and observations of the companion gamma ray at 100 TeV could clarify their intra or extragalactic origin. A wide FoV Cherenkov telescope could observe such event.

A wide FoV IACT system could also record events bellow the surface horizon that are originated by a τ neutrino EAS that decay into τ lepton.

The energy of such event would be between 100 TeV and 100 PeV.

To attain such wide FoVs a design based on the JEM-EUSO space telescope is proposed. The optic is composed of two double sided curved Fresnel lenses (Takahashi, Collaboration, et al., 2009). As recording device several POLAR camera modules could be used in order to cover a FoV of $60°$. POLAR is a gamma ray burst detector to be launched with the Chinese space station in 2016. It has a camera composed of multi-anode photomultipliers looking into a cube scintillating material. POLAR camera electronics triggers on fast (50 ns) flashes of ultraviolet photons. In the context of Cherenkov telescope scintillating bars are removed for light collection.

This design (see figure 1.2 and 1.3) developed at the INTEGRAL Science Data Centre (ISDC) in Geneva is tested under the night sky background conditions at the Geneva Observatory. Where the Fresnel lenses have a 1 m^2 collection area with a focal length of 2.4 m. The readout photomultiplier are multi-anode PMTs with 8×8 of 6×6 mm size (MAPM8500) from Hamamatsu. The angular resolution of the telescope optics is $0.13°$.

The following work is oriented on this telescope design and is based on CORSIKA version 74100 an air shower simulation program (Heck et al., 1998).

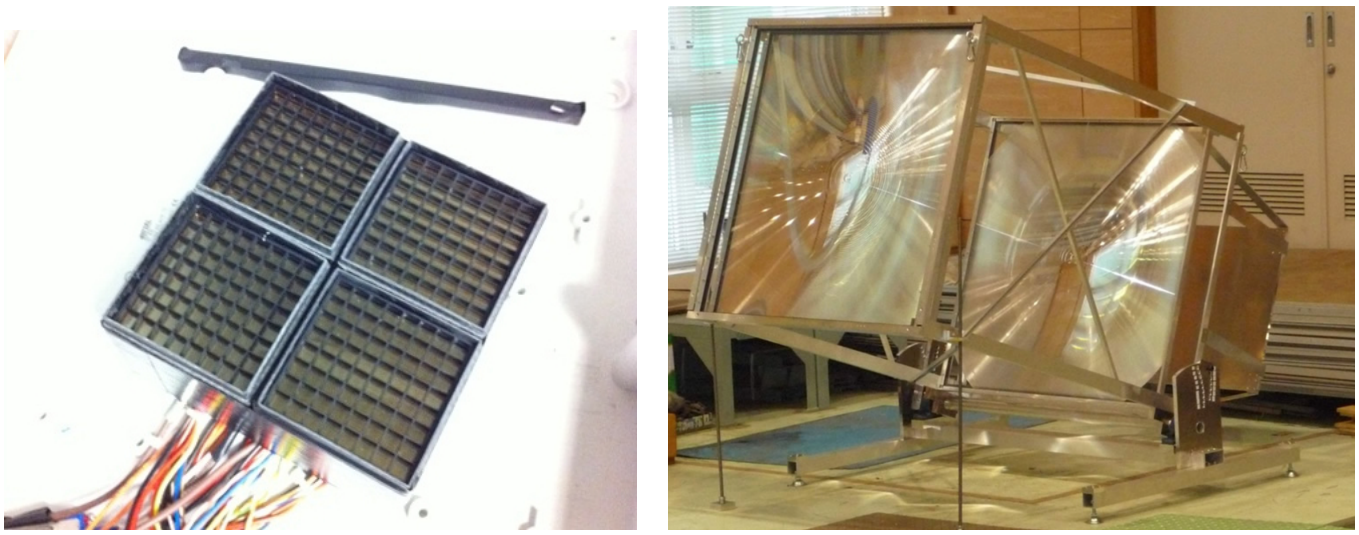

FIGURE 1.2: Camera module from POLAR (left) and telescope optic with Fresnel lenses (right).

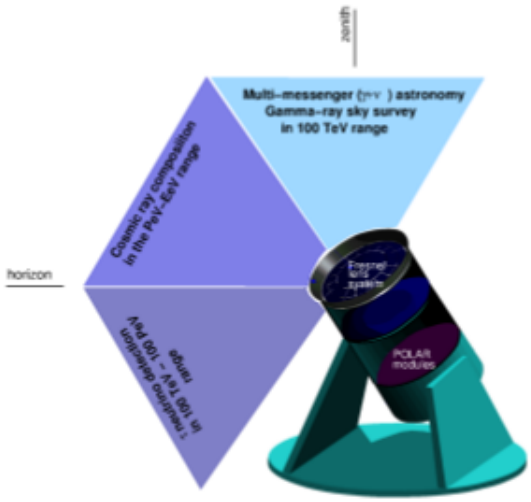

FIGURE 1.3: Wide FoV telescope possible observations.

1.4 Extensive air showers (EAS)

Extensive air showers are produced by an incoming cosmic ray particle interacting with the nucleus of an atom in the upper atmosphere producing numerous energetic hadrons which then would, as the primary particle, interact again with atmospheric nuclei or decay in the atmosphere.

To get a clearer picture of what is going on, extensive air showers can schematically be described by the following model (see figure 1.4). One can categorize EAS in two distinct categories: Electromagnetic showers and hadronic showers. The first is induced by a gamma, an electron or a positron that interacts with a nucleus in the atmosphere (N or O for instance) to create an electron-positron pair or a gamma. The electron and the positron will travel a certain distance before emitting a new photon. The new photons created will afterwards create an electron-positron pair and so forth. In the process of a hadronic shower several pions are produced. The charged pions will produce muons with muonic neutrinos while the neutral pion will produce a pair of gammas. The gammas produced will then generate an electromagnetic shower.

The shower particles are used to infer the properties of the primary cosmic ray by counting them with a detector. Some detectors use the electrons and muons produced by the pions disintegration reaching the ground, others use fluorescent light of the excited nitrogen of the atmosphere. The method of observation investigated in this work uses the Cherenkov light produced during the shower development.

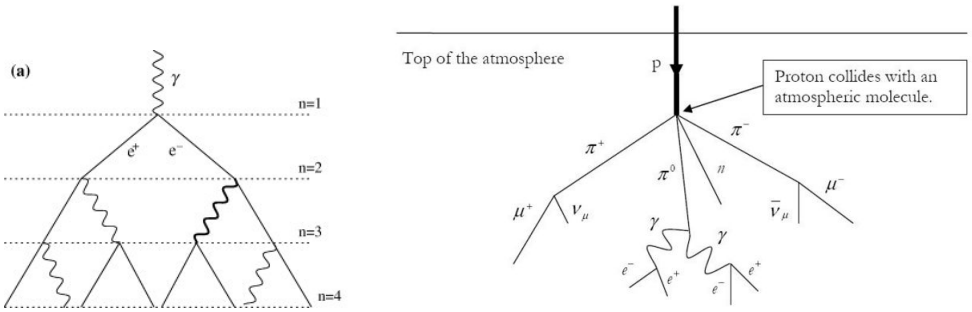

FIGURE 1.4: Electromagnetic (left) and hadronic (right) shower comparison. Source: Matthews, 2005 and *Comsic ray Wikipedia article*

1.4.1 Cherenkov light

Cherenkov light is emitted by a charged particle when it travels a dielectric medium faster than the speed of light in the medium. The discovery and interpretation of Cherenkov light awarded P. A. Cherenkov, I. Frank and I. Y. Tamm the 1958 Nobel Prize in Physics. This radiation is emitted at an angle θ from the direction of the particle. The angle is given by:

$$\cos\theta = \frac{1}{n\beta}, \tag{1.3}$$

where n is the refractive index of the medium and $\beta = \frac{v}{c}$ is the ration between the velocity of the particle v and the speed of light in vacuum c. From eq. 1.3 a cutoff eneregy can be defined at which the energy of the charged particle does not emit Cherenkov light anymore knowing that $\cos\theta \leq 1$:

$$\cos\theta \leq 1 \Rightarrow \beta_{min} = \frac{1}{n_{max}(h)} \Rightarrow E_{min} = \sqrt{\frac{1}{1 - n_{max}^{-2}(h)}} m_e c^2, \tag{1.4}$$

where m_e is the mass of the electron (i.e. electrons in EAS are the main contributors to Cherenkov light production) and where $n(h)$ is the refractive index which depends on the altitude h and can be expressed as (Bay, 2014)[p.70]:

$$n(h) = 1 + \delta = 1 + 2.9 \cdot 10^{-4} \exp\left(-\frac{h}{7.5[\text{km}]}\right). \tag{1.5}$$

Since $\delta \lll 1$ the minimum energy can be approximated by:

$$E_{min} \simeq \frac{1}{\sqrt{2\delta}} m_e c^2. \tag{1.6}$$

It gives a minimum energy at sea level ($h = 0$) of 21.2 MeV and of 95.3 MeV at 7.5 km altitude.

The Cherenkov light pool

As a result of eq. 1.3 and eq. 1.5 the maximum angle θ_{max} of emission as a function of the altitude is given by:

$$\theta_{max}(h) = \arccos\left(\frac{1}{n(h)}\right). \tag{1.7}$$

Thus the cone of emission is larger at detection level than at first interaction altitude. For instance, the maximum emission angle at sea level is $1.35°$ and $0.84°$ at 7.5 km. Therefore at sea level the Cherenkov photons are confined in an area of radius $r = h \tan\theta_{max}(h)$. For instance, at 7.5 km this radius ais bout 110.0 m. The area delimited by a radius $r_{pool} \simeq 110$ m is commonly referred as the Cherenkov light pool. Figure 1.5 shows the surface distribution of Cherenkov photons on the detection plane for a 1 TeV gamma showing the region of the light pool. For the gamma event the distribution is symmetric. The figure also shows the signal of a 1 TeV proton: several hot spots are present inside and outside the Cherenkov light pool. These spots are induced by muons created at early stages of the shower. Because most created muons do not decay in the atmosphere they produce Cherenkov light down to the ground level.

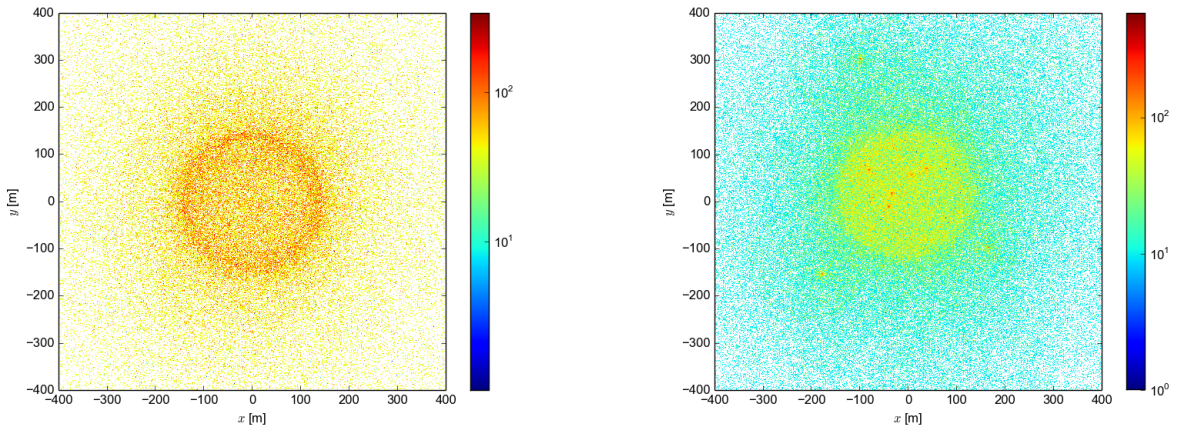

FIGURE 1.5: Surface distribution of a 1 TeV gamma (left) and a 1 TeV proton (right) shower coming perpendicularly to detection area. Distances are given in meters and the color map represents the number of Cherenkov photons on a logarithmic scale.

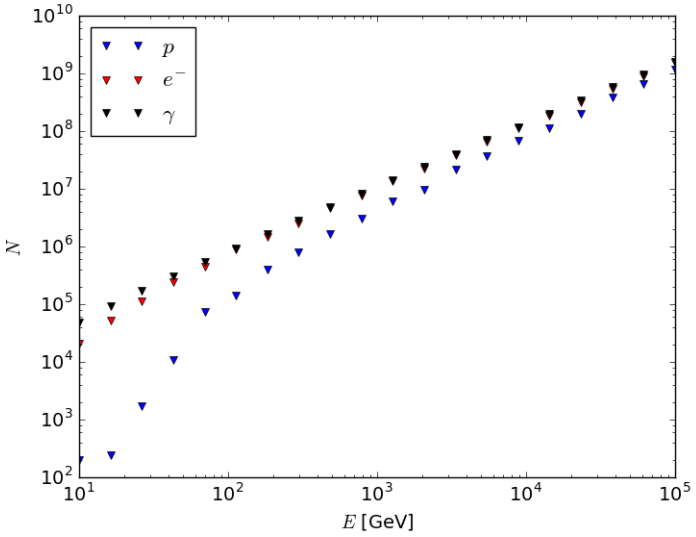

FIGURE 1.6: Number of Cherenkov photons as a function of primary energy.

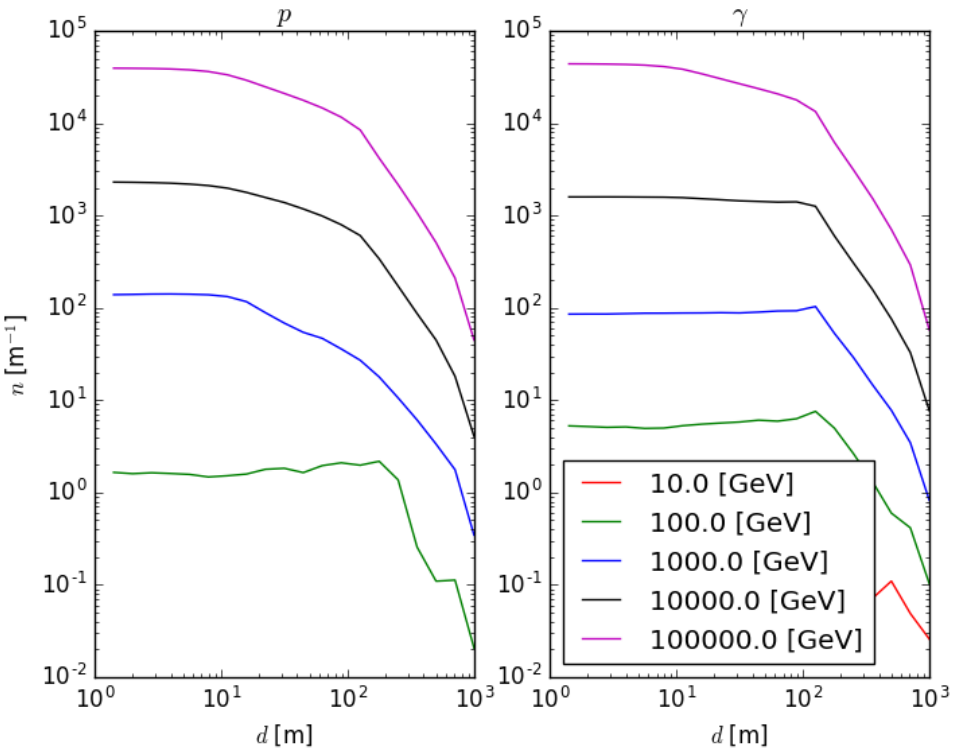

FIGURE 1.7: Longitudinal distribution for different energies.

Cherenkov light spectrum

The Cherenkov light spectrum is well defined by the Frank-Tamm formula:

$$\frac{\mathrm{d}^2 N}{\mathrm{d}\lambda \mathrm{d}x} = \frac{2\pi(ze)^2}{\hbar c}\frac{1}{\lambda^2}\left(1 - \frac{1}{\beta^2 n^2(\lambda, x)}\right), \tag{1.8}$$

where ze is the charge of the emitting particle in unit of electron charge, n the refractive index, λ the wavelength, x the path lenght and β the fraction of the speed of light. As one can see the spectrum starts at wavelengths λ such that $n(\lambda, x)\beta > 1$.

As a result Cherenkov light emitted in the atmosphere spectrum spread in the range $\lambda \in [250, 600]$ nm (*Cherenkov Radiation*). However Cherenkov light undergoes atmospheric absorption (see figure 1.8) thus the Cherenkov light spectrum peaks at 330 nm. In this region the night sky background spectrum is dominated by airglow (see figure 1.10). Therefore the maximum signal to noise ratio region is in $\lambda \in [330, 450]$ nm. Thus Cherenkov telescopes are equipped with filters in front of the camera that cut undesired wavelengths.

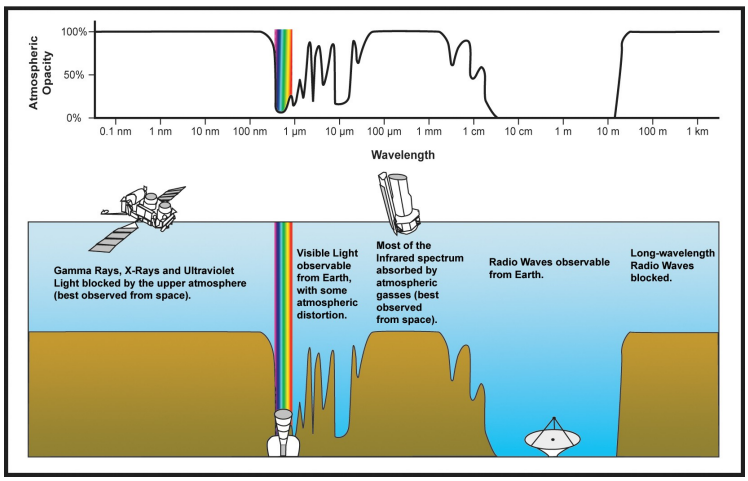

FIGURE 1.8: Atmospheric transmittance of the electromagnetic spectrum. Source : *Optical window Wikipedia article*

After undergoing absorption in the atmosphere the Cherenkov light will as well suffer from absorption in the telescope. At first the lenses will absorb part of the light. The transparency of the lens depends on the photon wavelength as well as the angle of incidence. For simplicity a constant lens transparency of 0.5 was considered.

When attaining the camera pixels the photons might not be always detected due to the quantum efficiency of photomultipliers. A quantum efficiency of 0.2 was considered.

1.4.2 EAS images and IACT technique

In the study of extensive air showers the direction (i.e where the source is located) and energy of the primary particle are the main parameters to recover. The number of Cherenkov photons collected in a detector depends on the altitude of first interaction, the distance to the center of the shower and the energy of the incident particle. Figure 1.6 shows the number of produced Cherenkov photons as a function of the energy. As one can see the number of generated Cherenkov photons in the cascade is proportional to the energy. Protons produce less Cherenkov light than electromagnetic particles because some energy is lost in the production of neutrinos and muons. At higher energies this difference is less important. At low energies a relatively small difference is observed between electrons and gammas.

On figure 1.9 on can see nine images of a 10 TeV electron over a 20m by 20m detection area. The center figure shows the electron shower from bellow the shower axis, this image would not look like most of images recorded in a telescope since it is perfectly located under the shower. However it is useful to see what happens to the image of the shower seen from several points of view. The eight other images show the same shower but seen from a distance of 100m at different locations around this radial distance. The almost perfect circle observed in the centred image now have a "comet" like shape and it points to the shower axis ($\theta = 0$). This observations show that if one has at least two images of the same shower at two different locations the source direction can be recovered. On figure 1.9 all "comets" point to $\theta = 0$ which is the direction of the source in the simulation.

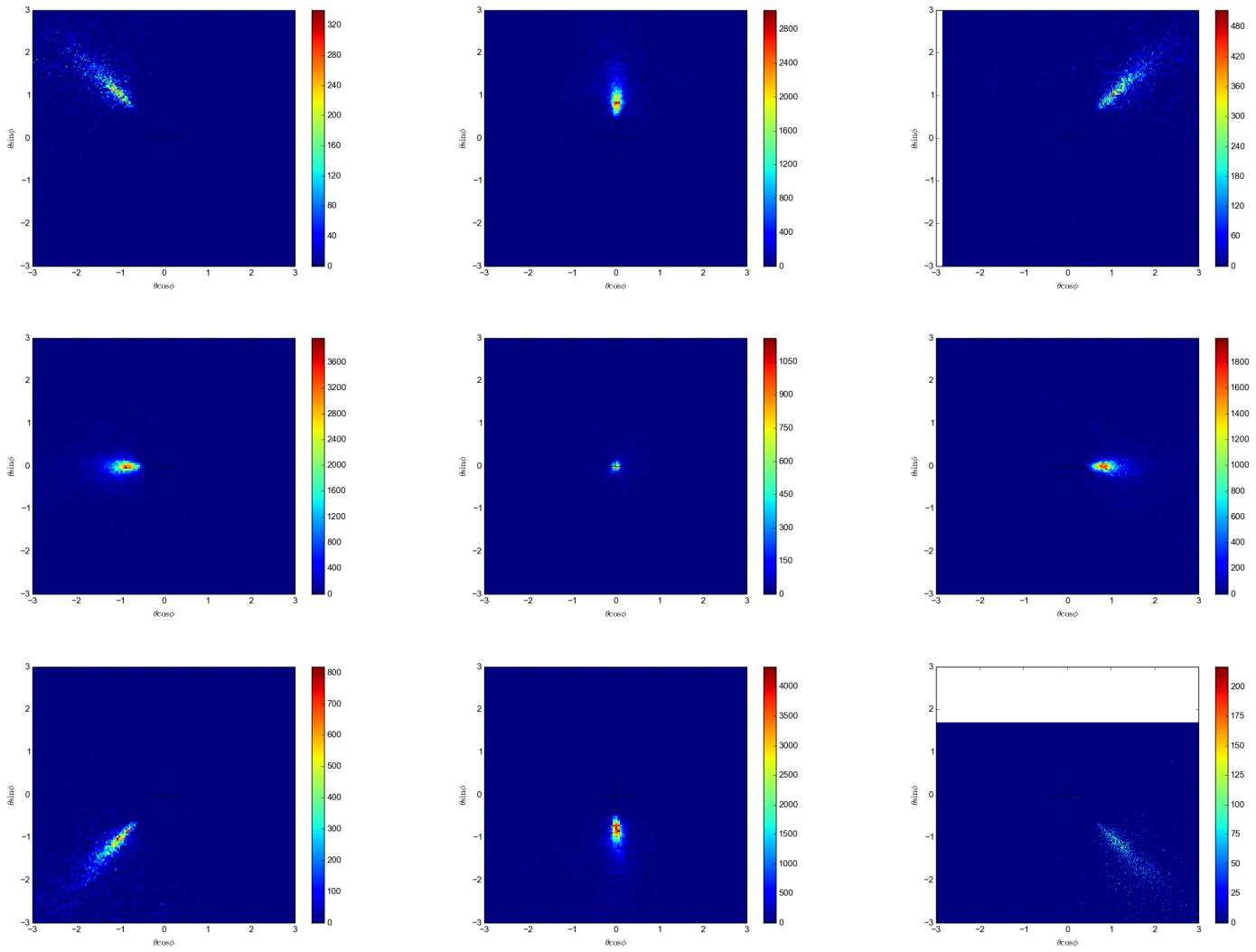

FIGURE 1.9: 10 TeV electron shower from a 20 m by 20 m detection area, the electron is coming perpendicularly to the telescope (i.e $\theta = 0$). The image at the center represents the shower image seen from below the electron direction. The other images show the same shower but viewed from a 100m distance in multiple directions (e.g the image in the top left corner is at $y = -x = 100/\sqrt{2}$m). The horizontal axis represents $\theta \cos\phi$ and the vertical axis represents $\theta \sin\phi$ where θ is the angle between the zenith and the incoming direction of the Cherenkov photon in the detector and where ϕ is the angle of the Cherenkov photon in the xy detection plane. All angles are given in degree. The values represent the number of Cherenkov photons.

1.5 Background noise

Cherenkov telescope imaging suffer as all imaging techniques in astronomy from noise. The noise level defines the detection threshold in energy of the primary particle as the number of Cherenkov photons produced is proportional to the primary energy (see figure 1.6).

The sources of noise are external or internal to the telescope. The internal noise is an electronic noise induced by random fluctuations in the electrical signals mostly due to the thermal effect. In MAPM each pixel could sense a cascade developing following a photon hit at certain place on the photocathode. However the cascade in one pixel could also "leak" into a neighbour pixel. This phenomenon would then induce a count overestimation of photons and is commonly referred as cross talk. In this work cross talk was ignored.

As a matter of fact any light induced by human activity such as public lighting (light pollution) is a source of noise in the telescope. Both electronic noise and light pollution can be reduced by choosing optimal instrumentation and by placing the telescopes in a remote area. However other sources of noises cannot be avoided.

Those unavoidable sources of noises are from the night sky background (NSB) and consist of the Moon, airglow, zodiacal light and star light. The Moon is a strong source of night sky background for instance a full moon night can increase the NSB up to a thousand times compared to a clear moonless night (Knoetig et al., 2013). This source of NSB can be avoided by observing during new moon phases.

Airglow is a phenomenon that emits light in the Earth's atmosphere. It causes the sky to never be totally dark. The atoms and molecules in the atmosphere are ionized by sunlight or cosmic rays when they recombine they reemit light. The oxygen and nitrogen present in the atmosphere might combine to form nitric oxide which will emit light as well. Airglow gives a bluish color to the night sky. (*Airglow Wikipedia article*).

Zodiacal light is a diffuse white glow that can be seen after sunset in spring and before sunrise in autumn. This glow is present along the ecliptic because it is caused by sunlight scattered by space dust. Thus the zodiacal light spectrum is similar to the spectrum of the Sun. (*Zodiacal light Wikipedia article*)

When pointing a telescope at the sky the stars that are not observed but are in the field of view (FoV) are sources of background in the telescope. Star light is mostly present in the galactic plane. However when pointing at a specific source the star light falling in the FoV is a point source that can be identified and removed.

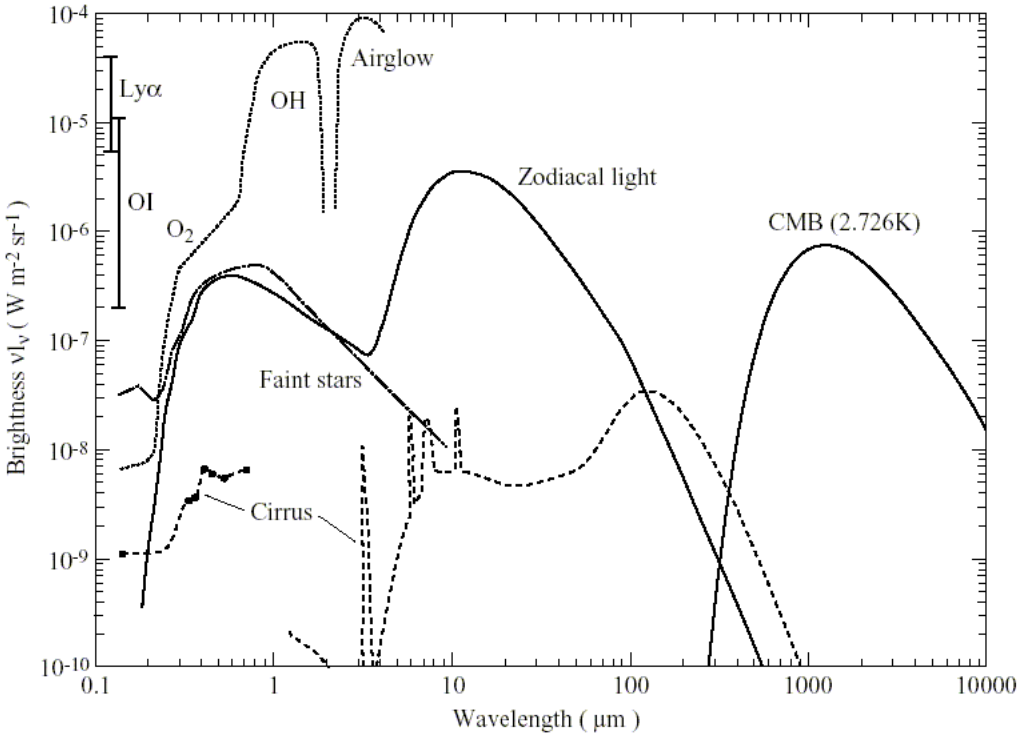

FIGURE 1.10: Night sky background spectrum. Source: Leinert et al., 1998

As Cherenkov light is in the ultraviolet range cameras are designed to detect such wavelength and to reject others. Therefore only UV emitters are sources. By looking at figure 1.10 the NSB rate per pixel can be computed. At 350 nm the brightness is about $2 \cdot 10^{-6}$ W m^{-2} sr^{-1} therefore the rate of NSB photons in a pixel λ_{NSB} is:

$$\lambda_{NSB} = 2 \cdot 10^{-6} \text{ W m}^{-2} \text{ sr}^{-1} = 1.25 \cdot 10^{13} \text{ eV m}^{-2} \text{ sr}^{-1} \text{ s}^{-1} \quad (1.9)$$

$$5.1 \cdot \text{ph m}^{-2} \text{ pixel}^{-1}\text{ns}^{-1} = 0.01 \cdot \text{ph m}^{-2} \text{ pixel}^{-1}\text{ns}^{-1}, \quad (1.10)$$

$$\lambda_{NSB} = 0.01 \cdot \text{ph m}^{-2} \text{ pixel}^{-1}\text{ns}^{-1}, \quad (1.11)$$

where a resolution of $(0.13)^2$ deg^2 was used.

The counting of NSB photons in each pixel is described by independent and identically distributed (i.i.d.) continuous time Poisson process $N(t)$ of parameter λ given by the following distribution:

$$P(N(T+t) - N(t) = k) = \frac{(\lambda T)^k}{k!} e^{-\lambda T}, \ \forall t, T > 0 \text{ and } \forall k \in \mathbb{N} \quad (1.12)$$

It express the probability in any time interval of length T that k photons are in a pixel. The sequences of arrival are given by exponential i.i.d. random variables of mean $1/\lambda$ where the probability density function is:

$$f(t) = \lambda e^{-\lambda t}, \ t \geq 0 \quad (1.13)$$

Chapter 2

Results: Characteristics of refractor wide FoV Cherenkov telescope at Geneva observatory

2.1 Time of arrival of Cherenkov light

Cherenkov light produced in extensive air showers can generate a bright event in the telescope up to 30000 ph. m^{-2} for 100TeV as can be verified on figure 1.7. However those photons are emitted during short times. It means that a Cherenkov telescope should be equipped with a fast trigger system. The results presented in this section aim to study the time of arrival of Cherenkov light in the telescope the trigger and readout system camera on the impact of the details of image reconstruction of an extensive air shower.

As a first calculation the following representation gives a good approximation of the time spread between first and last arrival of Cherenkov photons. Consider an angle of emission θ at altitude h. Then the surface at sea level illuminated by the Cherenkov light is a circle of radius $r = h \tan\theta$ (see figure 2.1). Thus the time spread of photons Δt is:

$$\Delta t = \frac{r \sin\theta}{c_{air}} = \frac{h \tan\theta \sin\theta}{c_{air}}, \text{ with } c_{air} = \frac{c}{n} \tag{2.1}$$

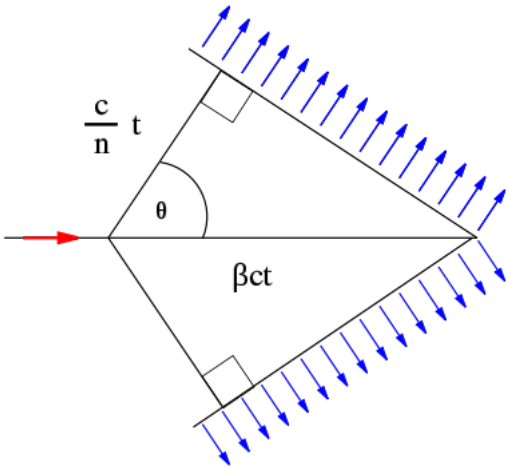

FIGURE 2.1: Cherenkov radiation schematic. Source: *Cherenkov radiation Wikipedia article*

In fact as mentioned in section 1.4.1 the emission angle θ depends on the altitude h. This approximation considers one charged particle travelling along the shower axis; however many particles are produced in the shower that can travel along different trajectories resulting in larger emission angles.

Studying the time of arrival of Cherenkov photons in a telescope is of great importance in order to reduce background in the images. Using a large time of aperture in the camera would assure that most Cherenkov photons from the shower are collected, but it also increases the number of NSB photons captured. Figure 2.2 gives a differential and a cumulative distribution of the time of arrival of photons in an area of radius $r = 120$ m and $r = 1$ km as deduced from CORSIKA simulation runs. The value t_{90} is defined as:

$$t_{90} = \max_{0 \leq N \leq 0.9 N_{max}} t\left(N\right), \tag{2.2}$$

where N is the number of photons in the area of delimited by the radius r.

It confirms that in the light pool ($r \leq 110$ m) Cherenkov light arrives in shorts times (i.e. $t_{90} = 8.2$ ns for gamma rays) and that at further distances the time spread t_{90} becomes larger (i.e. $t_{90} = 140.4$ ns for gamma rays with $r = 1$ km). This has important implications for the optimization of the camera trigger system. Choosing a narrow trigger time window (e.g. $\Delta t = 10$ ns) like in existing Cherenkov telescopes (Magic, HESS, Veritas) one reduces the NSB, but also looses signal from distant EASs. A large time window assure detection of distant showers at the expense of high NSB.

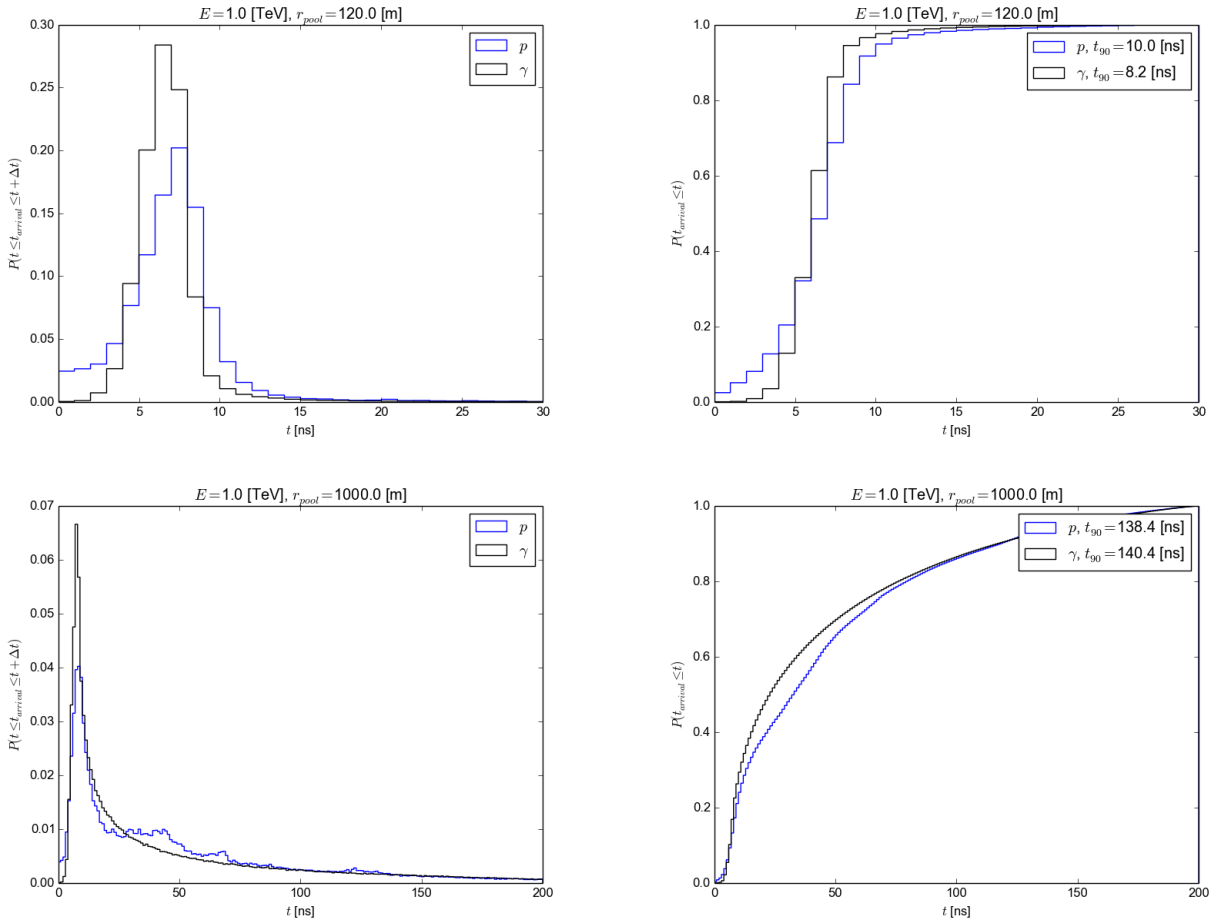

FIGURE 2.2: Probability density (left) and cumulative distribution (right) of time of arrival of Cherenkov light for a gamma and a proton shower at 1 TeV. In the simulation an area of radius $r = 120$ m (top) and $r = 1$ km (bottom) centered at shower axis is considered.

Figure 2.2 shows the arrival time of Cherenkov photons in a large area however in reality there is no Cherenkov telescope with such huge collection area. But ground based telescopes are usually arranged in array of detection which means that observers separated by long enough distances would trigger the same shower at different times.

2.1.1 Time spread of Cherenkov light in the telescope

The time spread of arrival of photons in a single telescope can be wide at further distances from the shower axis. An image of an extensive air shower would have the form of a "comet" in the telescope. For a shower observed at a longer distance from the shower axis the "comet" would actually be longer in terms of angular size than at closer distance from the shower axis as shown on figure 2.3. In order to explain that the length of the "comet" is wider at larger distances it is to be understood that an observer situated closer to the shower axis is seeing the shower from above and thus will see photons in a narrow cone compared to the outer observer which is seeing the shower from the side and thus has a vaster cone of view.

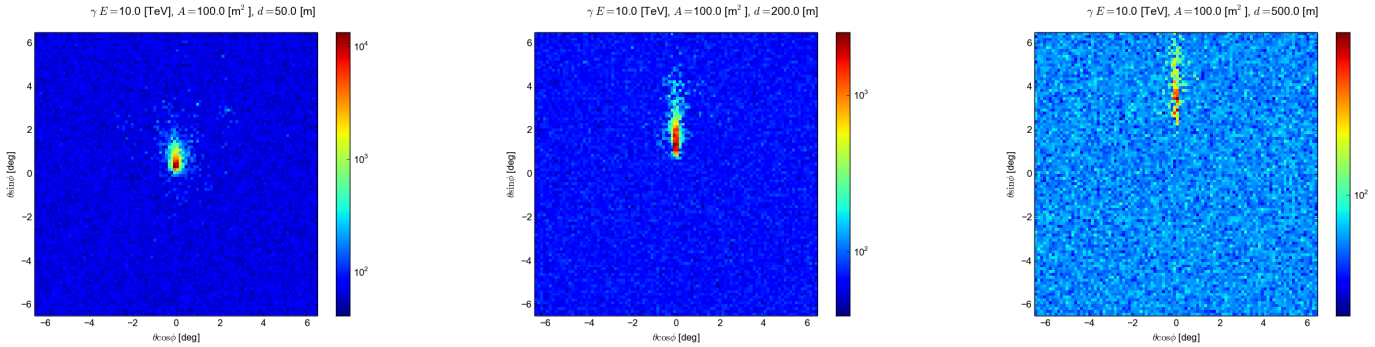

FIGURE 2.3: Image of a 10 TeV gamma ray shower in a telescope of 100 m^2 at (from left to right) $d = 50$ m, $d = 200$ m and $d = 500$m.

Hence the time that a photon takes to travel from the top of the shower to the telescope is a bit shorter that the time it takes for a photon from the bottom of the shower. And this difference of time becomes larger when the observer is further from the shower axis.

On figure 2.4 a 10 TeV gamma ray event is shown at three different times $t = 2$ ns, $t = 5$ ns and $t = 10$ ns from a telescope situated at 200 m from the shower axis. The images show that the shower develops from low angles to large angles of emission θ. Thus an event that is triggered at very early stage of the shower development in the telescope would result in missing count of Cherenkov photons in the images which would result in a lower energy estimation.

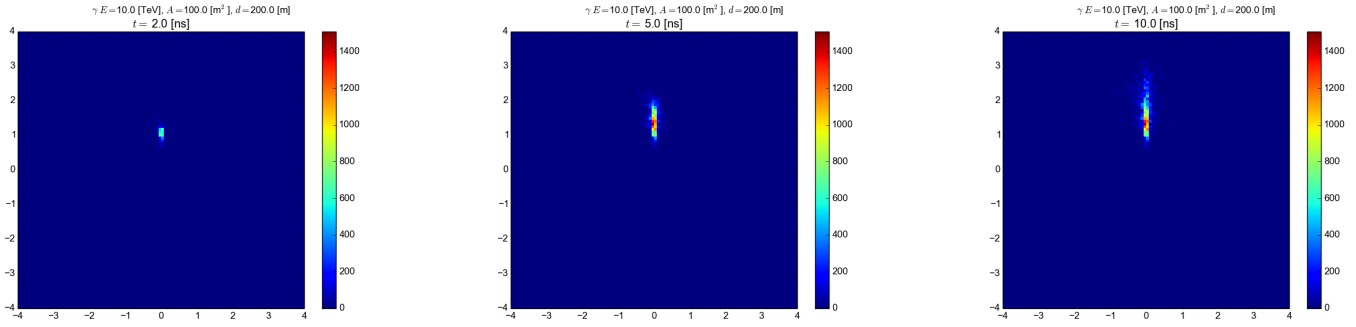

FIGURE 2.4: Development of a gamma ray shower at 10 TeV in a telescope of 100 m^2 at different times t since first arrival (form left to right) $t = 2$ ns, $t = 5$ ns and $t = 10$ ns and at distance $d = 200$ m from the shower axis.

On figure 2.4 the time spread between the first and 90% of photons is about $t_{90} \simeq 10$ ns. However the triggering system of POLAR camera would not react on such short time scale. Nevertheless the bias on energy resolution could be more important when observing at larger distances than 200 m. On figure 2.5 the time spread t_{90} is shown as a function of the distance to shower axis d. The value of t_{90} is the mean of 20 different proton showers at 1 TeV. It shows that the time spread remains constant inside the light pool (i.e. 8 ns) and then starts increasing at a distance of 200 m up to 300 ns at 1 km.

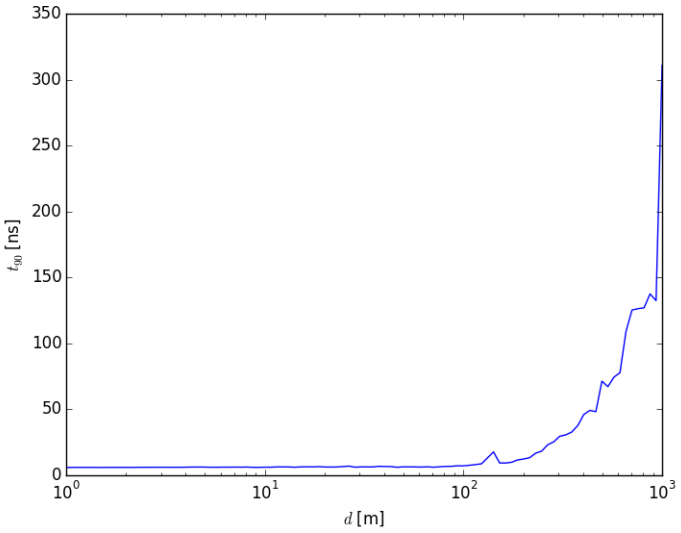

FIGURE 2.5: t_{90} as a function of the distance d to the shower axis for a 1 TeV proton shower.

2.1.2 Study of the trigger of POLAR camera

To avoid bias in energy estimation the aperture time of the camera should be taken large enough but as mentioned above time during which Cherenkov photons are counted should not be too big otherwise the night sky background in the telescope would increase the trigger level and thus lower the energy threshold of the telescope.

The camera triggers when either one or several pixels exceed a threshold. The signal which is compared with the threshold is the PMT pixel signal convolved with a shaping function following the trigger values in each pixel are stored and red out by an Analog to Digital Converter (ADC). The case where multiple pixel triggers exceed the threshold is not studied.

By setting that recording at least 90% of Cherenkov light (without taking into account quantum efficiency and reflectivity) is a condition for good enough image reconstruction, figure 2.5 is the basis to choose. For aperture times greater or equal to 100 ns there should be no impact on the energy estimation. Note that at distances larger than 500 m the night sky background dominates the signal of the shower (see bellow).

In order to study the missing count of photons in the telescope due to the time spread of arrival the following simulation of a realistic trigger system was considered. Each input signal in a PMT pixel is connected to a signal shaper with impulse response $g(t)$:

$$g(t) = \frac{t}{\tau} \exp\left(1 - \frac{t}{\tau}\right). \tag{2.3}$$

If t_i are the time of arrival of each photons (Cherenkov photons and NSB photons) in the detector then the input signal $x(t)$ is:

$$x(t) = \sum_i a_i \delta(t - t_i), \tag{2.4}$$

where a_i is the number of photons arrived at time t_i and $\delta(t)$ the Dirac delta function.

The output signal $y(t)$ going out of the shaper is then:

$$y(t) = (x * g)(t) = \int_{-\infty}^{\infty} \sum_i a_i \delta(t' - t_i) \frac{t - t'}{\tau} \exp\left(1 - \frac{t - t'}{\tau}\right) \mathrm{d}t', \tag{2.5}$$

$$y(t) = \sum_i a_i \frac{t - t_i}{\tau} \exp\left(1 - \frac{t - t_i}{\tau}\right). \tag{2.6}$$

The parameter τ is called the time of rise i.e. the time it takes for the shaped signal to rise to the maximum value. The impulse response of the filter satisfies $g(t) \leq 1 \; \forall t$ thus the output signal $y(t)$ gives the counted value of photons in a time window of $\Delta t = \tau \exp(1)$. Where the value Δt is computed by comparing $g(t)$ with a box function.

In order to trigger an event and assure that the event is not due to the night sky background fluctuations in the detector, a detection threshold is used. In the simulation each pixel is able to trigger an event if its value is above a 5σ level. When one of the pixel records a value above the trigger threshold it orders the telescope to record the values in every pixel. From the time that the output signal reaches a 5σ level ($t_{reaction}$) and the time that the value is recorded there is a short delay time t_{delay} due to the electronics. Therefore the electronics in the telescope has to be designed such that the time of reaction plus the time of delay is equal the rising time in order to record the maximum possible count (i.e. $\tau \simeq t_{reaction} + t_{delay}$).

As mentioned above the threshold is at a 5σ level above the mean NSB value. For a telescope of collecting area A, a filter with impulse response $g(t)$ as in equation 2.3 and a field of view Ω with N^2 pixels, the mean NSB output value $\langle y(t) \rangle$ is:

$$\langle y(t) \rangle = \langle y \rangle = \lambda_{NSB} A \left(\frac{\Omega}{N}\right)^2 \tau \exp(1). \tag{2.7}$$

The threshold is fixed at $5\sigma + \langle y \rangle = 5\sqrt{\langle y \rangle} + \langle y \rangle$.

On figure 2.6 the signal of a 1 TeV gamma ray in the brightest pixel is shown for a NSB rate of $\lambda = 0.01$ ns^{-1} m^{-2} pixel^{-1}. The telescope has a collecting area $A = 100$ m^2(as an example) a pixel angular size of 0.13^2 deg^2, a rising time $\tau = 25$ ns and a delay time $t_{delay} = 20$ ns. In this case the mean night sky background count is 68 ph. pixel^{-1} which gives a threshold at 109.2 ph. pixel^{-1}. The simulation were done over a 2000 ns window of time in which night sky background is simulated according to equations 1.12 and 1.13. The time zero is set at the time at which the first photon arrives at the pixel. The blue dashed line represents the time at which a count value is recorded. It shows that the telescope was able to respond

fast enough in order to get a value close to the peak maximum (i.e. in 28.4 ns where the maximum value is at $\tau = 25$ ns).

However this is not certainly the case in each pixel since as discussed in section 2.1.1 the photons can arrive at well separated time intervals. Hence the peaks in each pixels would be shifted in time compared to the peak in the pixel that triggered the event and would result in a lower estimation of the Cherenkov light count.

This effect is shown on figure 2.7 where on the left plot the output signal is given for 7 pixels along the image axis. The labels give the pixel situation [i,j] in the image $N \times N$ matrix where the origin is situated in the left top corner. The i index represents the vertical axis while the j axis represents the horizontal axis. The y-scale is logarithmic for clearness. The purple line gives the signal in the pixel that triggered the event since it starts rising at $t = 0$. For this pixel there is almost no missing in the count since the time of acquisition $t_{acquisition} \simeq \tau = 25$ ns however for the other curves there is small underestimation of the Cherenkov photon count. Next to the pixel signals an image of the simulated shower used is displayed. The shower is a 10 TeV gamma ray event in a telescope of 100 m^2 situated at a distance $d = 300$ m from the shower axis.

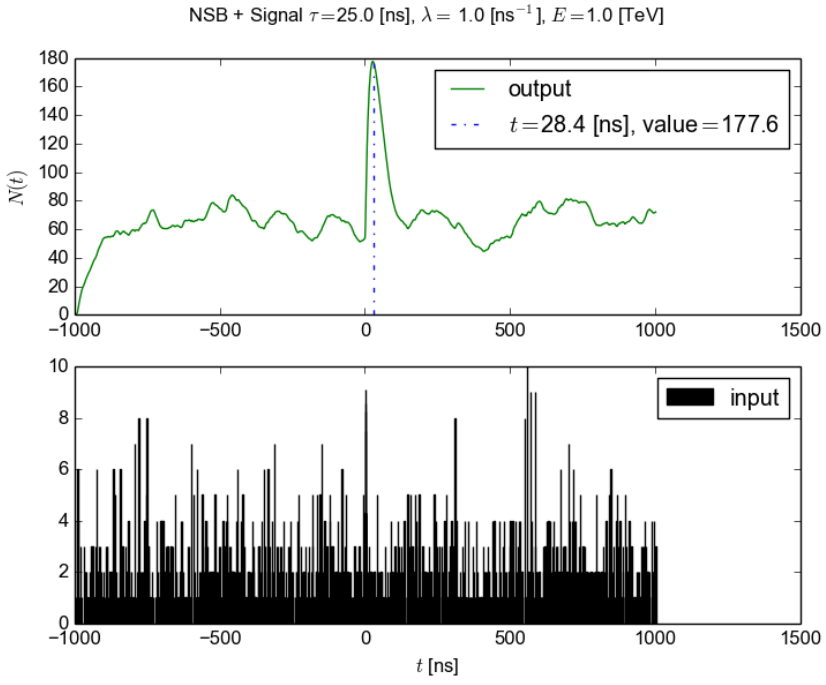

FIGURE 2.6: Output signal of the system (top) and input signal (bottom) with night sky backgroud rate $\lambda = 0.01$ ns^{-1} m^{-2}.

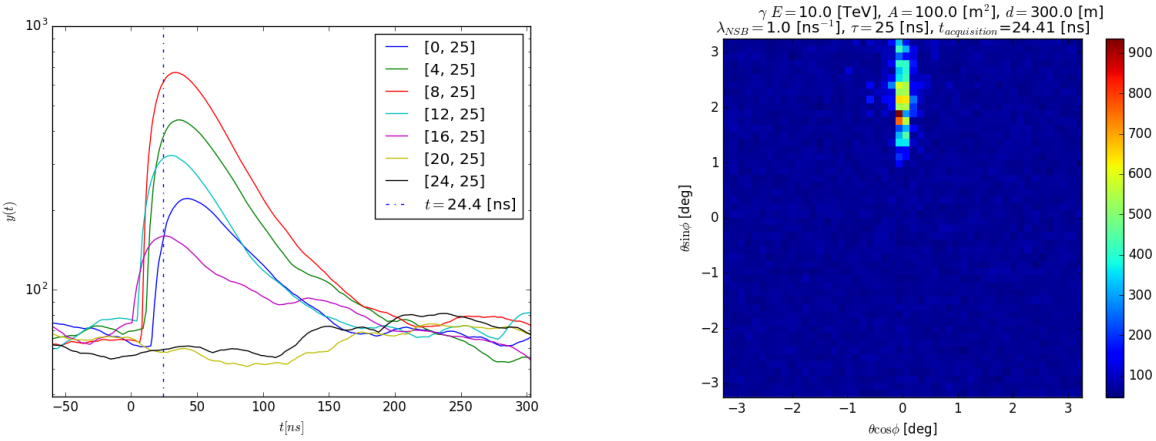

FIGURE 2.7: Output signal $y(t)$ for several pixels along the image axis (left) and the corresponding image obtained of the shower (right).

On figure 2.8 is shown the count of photons along the image axis at $\phi = \frac{\pi}{2}$ for the case where the image is triggered (red) and for the case where the image is taken from an ideal telescope (blue). The ideal telescope does not take the time of arrival into account and each pixel contains an additional NSB similar to the NSB in the other telescope. The simulation were done for a telescope of area $A = 400$ m^2 and a NSB at $\lambda_{NSB} = 0.01$ ph. ns^{-1} m^{-2} pixel^{-1} with rising time $\tau = 25$ ns. The results are given for two different distances from the shower axis $d = 300$ m (top) and $d = 500$ m. As it should be expected the red bins should be always bellow the blue bins because the ideal telescope counts more Cherenkov light than the telescope with the trigger system. However in the figures it is not always the case, this is due to the superposition of randomly distributed night sky background. For the telescope with the trigger, the night sky background is generated over time following equations 1.12 and 1.13 where for the second telescope the NSB is generated through a single value in each pixels. At $d = 300$ m the counting of photons is not drastically affected by the triggering since the difference between the two graphs is not relatively large. However at a further distance of $d = 500$ m the difference starts to be significant. But at 500 m we see that the maximum value (375 ph.) starts to be at the threshold level of $250 + 5\sqrt{250} \simeq 329$ photons. It means that the underestimation of photon count starts to be important at distances at which the detection limit is reached and thus that this effect could be negligible.

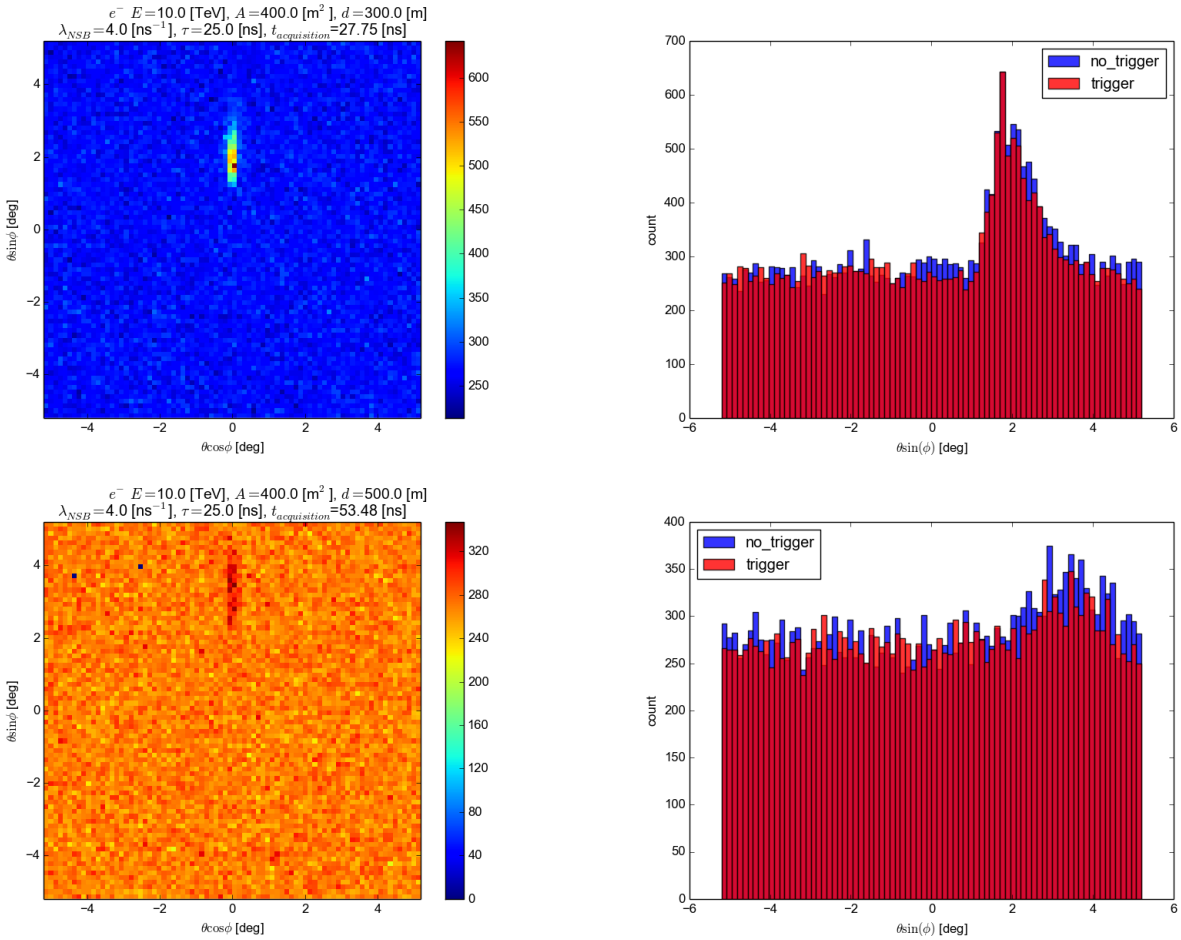

FIGURE 2.8: Image reconstruction with trigger condition at 5σ for an electron shower at 10 TeV at 300 m (top) and 500 m (bottom). Compared pixels values along image axis with number of generated photons (blue) and counted photons (red).

2.2 Effective area

In gamma ray astronomy the flux of photons from astronomical sources is expressed in photons per cm^2 per second per energy bin. In order to measure the flux the observer has to count the number of events at a certain energy over a period of time. But the telescope the observer uses is not capable to record each events from the source. The fact that the telescope does not record each events is explained by different factors. The first and obvious one is that the event is not detectable because the energy of the event is weak thus the signal to noise ration is too low. The second can be explained by the fact that the telescope is situated far away from the shower axis. As a third reason it could be that the telescope is still recording a previous event therefore it is occupied and would miss an extensive air shower.

In order to resolve this issue of missing events in the telescope the observer should be aware of the effective area A_{eff} of the telescope. Then the

flux of the source $\Phi(E)$ as a function of the energy E is given by:

$$\Phi(E) = \frac{N_{events}(E)}{A_{col}T_{obs}} = \frac{N_{obs}(E)}{A_{eff}(E)T_{obs}}, \tag{2.8}$$

where N_{obs} is the number of counted events and N_{events} is the true number of events generated by the source, A_{coll} is the area on the ground in which Cherenkov light is collected and T_{obs} the observation time. From equation 2.8 the formulation of the effective area becomes:

$$A_{eff}(E) = A_{coll}\frac{N_{obs}(E)}{N_{events}(E)}. \tag{2.9}$$

2.2.1 Computation of effective area with Monte Carlo

In order to compute the effective area of a telescope 30 showers for 20 energies logarithmically spaced from 10 GeV to 10^5 GeV where generated over a square collection area of surface A_{coll} in which N telescopes of detection surface A were placed randomly. The telescope was placed randomly in this area according to a uniform distribution in x and y. The effective area is then computed with equation 2.9 where one counts the number of observed events. In order to compute reasonably well the effective area the number of placed telescope N should be set at more or less 1% of the ratio between the collection area the telescope area i.e. $N \simeq 0.01\frac{A_{coll}}{A}$. Unless varying the default values presented in table 2.1 were used in the computation of the effective areas.

A [m^2]	A_{coll} [m^2]	λ_{NSB} [ph. ns^{-1} m^{-2} pixel^{-1}]	FoV [deg]	τ [ns]
1	$1.6 \cdot 10^5$	0.01	9.88	25

TABLE 2.1: Default values used for the computation of effective areas.

Due to computational limits all Cherenkov photons produced in the simulation cannot be recorded without taking enormous space in the hard drive. To give an order of magnitude *CORSIKA* stores photons in bunches of size 50 by default and each bunch has 7 informations encoded for each 4 bytes are needed. Thus a single photons takes on average 0.56 byte of disk space. By looking at figure 1.6 the number of photons for 10 TeV shower reaches billions. In fact it is more since the number of photons where counted only in the light pool. Therefore files can reach 50GB of disk space.

To avoid having to much data to analyze an energy cutoff of particles in the shower was chosen. It is the energy at which secondary particles are no longer tracked and therefore do not produce Cherenkov light anymore. For hadrons and muons $E_{cut} = 0.3$ GeV while for electrons and photons $E_{cut} = 0.1$ GeV. But to reduce more significantly the disk space a collection area has to be defined. In reality the collection area is bounded by Earth's geometry however it represents too much of a surface for the simulation. On the other hand if one chooses a collection area too small

the effective area computed would be bounded by the collection area (as shown on equation 2.9).

On figure 2.9 the effective area as a function of the primary particle energy is computed for different collection area of surface A_{coll}. This computation was done in order to identify which area of collection should be taken in order to avoid a plateau of the effective area.

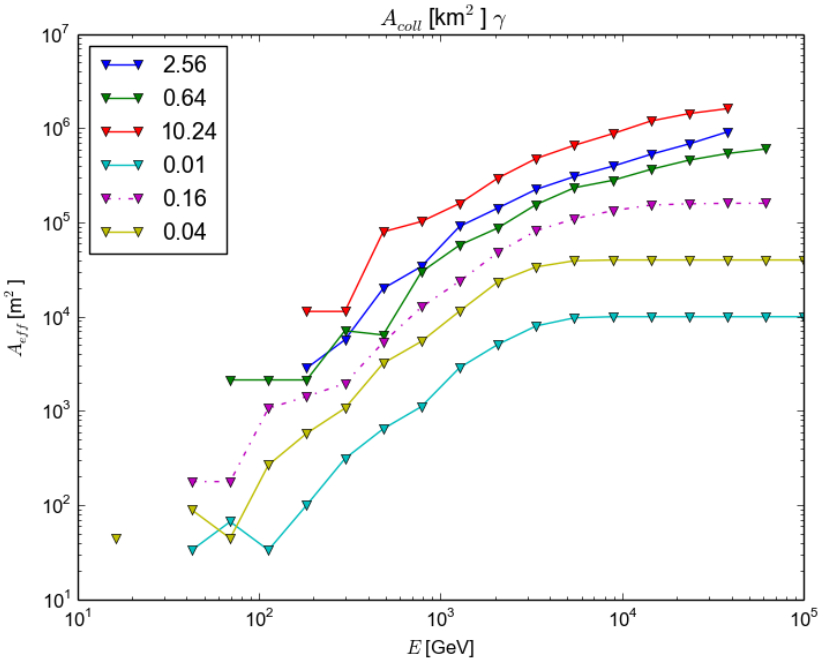

FIGURE 2.9: Effective area as a function of the collection area A_{coll} in km^2.

2.3 Effective areas varying telescopes size and night sky background

Here is presented the results obtained for effective areas as functions of the detection surface A and the night sky background rate λ_{NSB} for gamma ray showers. As disused in section 1.5 the night sky background level defines a minimum detection energy. This level increases proportionally to the surface of detection of the telescope. Meaning that if one has a larger telescope one collects more NSB photons as well.

Figure 2.10 shows the telescope effective area as a function of energy. One could define the energy threshold at the energy where the curves starts because at those points no events where triggered from the simulation. From this figure we conclude that for a telescope of 1 m^2 the energy threshold is around 100 GeV for a night sky background rate $\lambda_{NSB} = 0.01$ ph. ns^{-1} m^{-2} pixel^{-1}. One can see that the effective areas curves are linearly spaced in the low energy regions. For larger telescopes the sensitivity to lower energies is obviously increased but reaches its limits for enormous

telescope of area $A \geq 1024$ m^2. While larger telescopes are more sensitive to low energies than small telescopes.

The energy threshold could be defined as the energy at which close to 100 % of the showers become detectable within the Cherenkov light pool (i.e $rsimeq110$ m).

For a telescope of 256 m^2 the energy threshold is around 100 GeV which correspond to MAGIC. To the contrary, the 1 m^2 telescope at the roof of Geneva observatory has much higher energy threshold in the 10 TeV range. This makes observations of gamma ray sources with this design impossible because of the too low signal statistics at 10 TeV. However the Geneva observatory setup could still be used for testing the observation techniques of wide FoV refractor telescopes. The detectable air shower energies are above 10 TeV. From figure 1.1 and figure 2.10 an event rate could be estimated at about 17 events per second in a steradian wide FoV knowing that the cosmic ray flux is around 10^{-7} m^{-2} s^{-1} sr^{-1}.

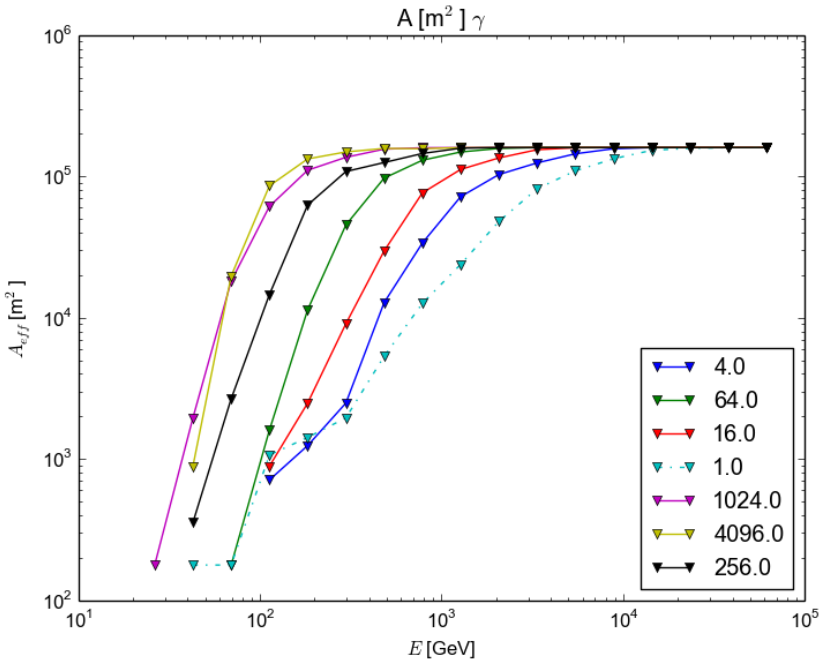

FIGURE 2.10: Effective area as a function of the telescope area A in m^2.

On figure 2.11 is presented the effective area as a function of the energy for different night sky background rates. As expected the NSB level increases the energy threshold as it increases. It also decreases the sensitivity in the detectable energy regions. For the default configuration (dashed) the energy threshold around 100 GeV which is the La Palma night sky conditions under a clear moonless night. But as mentioned in section 1.5 the NSB can reach a thousand time its regular value on full moon night. Conditions which would correspond to a NSB rate $\lambda_{NSB} = 10$ ph. ns^{-1} m^{-2} pixel^{-1} therefore the energy threshold is around 20 TeV which makes observations

quite difficult.

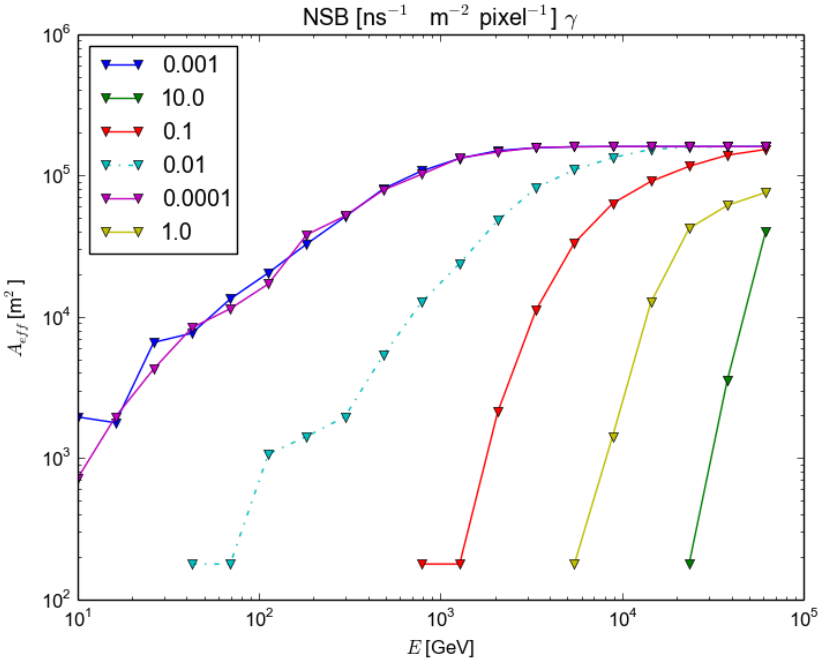

FIGURE 2.11: Effective area as a function of NSB in ns^{-1} m^{-2} pixel^{-1}.

At the Geneva observatory the NSB is comparable to a moderate half-moon light. Which corresponds to a NSB rate $\lambda_{NSB} = 0.1$ ph. ns^{-1} m^{-2} pixel^{-1}. Under such circumstances one can conclude from figure 2.11 that the energy threshold is around 10 TeV. At this energy the effective area is small. Nevertheless at higher energies the high NSB does not affect detection of showers.

Chapter 3

Conclusion

This project was undertaken to evaluate the differences between observed EAS and emitted EAS for a defined triggering system. As well as to determine the effective area of a wide FoV Cherenkov telescope under various noises conditions in order to foresee its energy threshold at the Geneva observatory.

The results of this investigation show that the trigger system of POLAR is able to recover photon count well for distances up top 500 m from the shower axis. Above 500 m the counting of photons is affected by the time spread of Cherenkov light. The study of effective areas has shown that the wide field telescope energy threshold is around 100 GeV for gamma rays under regular night sky background conditions. Moreover the energy threshold of the telescope is at 1 TeV if the night sky background rate is 10 times higher. From the results it is established that a larger telescope increases considerably the sensitivity in the energy range bellow 1 TeV but above this energies a small size telescope would perform well.

These findings suggest that the 1 m^2 wide FoV Cherenkov telescope will have good sensitivity in the energy above 100 TeV which corresponds to the minimum energy for the forecasted studies.

The most important limitation lies in the fact that the simulation of the telescope does not take into account a realistic lens transparency and quantum efficiency of the SiPM. Due to computational limits, the computation effective areas was done on not large enough collection areas. The study did not consider cross talk and dark counts in MAPMs.

Further studies could be done on the impact of the lenses transparency in the computation of effective area. The impact on energy resolution due to an underestimation of Cherenkov light and its impact on energy determination should be studied beyond. To further reduce energy bias one could study a trigger system with multiple local triggers dispatched on the camera. Finally it would be interesting to test a background rejection with EAS simulations.

Bibliography

Acharya, BS et al. (2013). "Introducing the CTA concept". In: *Astroparticle Physics* 43, pp. 3–18.

Airglow Wikipedia article. https://en.wikipedia.org/wiki/Airglow. Accessed: 2016-06-17.

Bay, A. (2014). *Introduction aux astroparticules*.

Benn, Chris R. and Sara L. Ellison. *La Palma Night-Sky Brightness*. http://www.ing.iac.es/Astronomy/observing/conditions/skybr/skybr.html. Accessed: 2016-06-17.

— (2007). *La Palma night-sky brightness, La Palma technical note 115*.

Cherenkov Radiation. http://www.gae.ucm.es/~emma/docs/tesina/node4.html. Accessed: 2016-06-17.

Cherenkov radiation Wikipedia article. https://en.wikipedia.org/wiki/Cherenkov_radiation. Accessed: 2016-06-17.

Comsic ray Wikipedia article. https://en.wikipedia.org/wiki/Cosmic_ray. Accessed: 2016-06-17.

Gaug, M. and f. t. CTA Consortium (2013). "Night Sky Background Analysis for the Cherenkov Telescope Array using the Atmoscope instrument". In: *ArXiv e-prints*. arXiv: 1307.3053 [astro-ph.IM].

Gaug, Markus et al. (2013). "Night Sky Background Analysis for the Cherenkov Telescope Array using the Atmoscope instrument". In: *arXiv preprint arXiv:1307.3053*.

Haungs, A. et al. (2015). "KCDC - The KASCADE Cosmic-ray Data Centre". In: *J. Phys. Conf. Ser.* 632.1, p. 012011.

Heck, D. et al. (1998). *CORSIKA: a Monte Carlo code to simulate extensive air showers.*

Knoetig, M. L. et al. (2013). "FACT - Long-term stability and observations during strong Moon light". In: *arXiv:1307.6116 [astro-ph]*. URL: http://arxiv.org/abs/1307.6116 (visited on 01/06/2016).

Leinert, Ch et al. (1998). "The 1997 reference of diffuse night sky brightness". In: *Astronomy and Astrophysics Supplement Series* 127.1, pp. 1–99.

Matthews, J (2005). "A Heitler model of extensive air showers". In: *Astroparticle Physics* 22.5, pp. 387–397.

Optical window Wikipedia article. https://en.wikipedia.org/wiki/Optical_window. Accessed: 2016-06-17.

Stanev, T. (2003). *High Energy Cosmic Rays*. Springer-Praxis.

Swordy, S.P. (2001). "The Energy Spectra and Anisotropies of Cosmic Rays". English. In: *Space Science Reviews* 99.1-4, pp. 85–94. ISSN: 0038-6308. DOI: 10.1023/A:1013828611730. URL: http://dx.doi.org/10.1023/A%3A1013828611730.

Takahashi, Yoshiyuki, JEM-Euso Collaboration, et al. (2009). "The Jem-Euso Mission". In: *New Journal of Physics* 11.6, p. 065009.

Weekes, Trevor C et al. (1989). "Observation of TeV gamma rays from the Crab nebula using the atmospheric Cerenkov imaging technique". In: *The Astrophysical Journal* 342, pp. 379–395.

What Are Cosmic Rays. http://www.telescopearray.org/index.php/about/what-are-cosmic-rays. Accessed: 2016-06-17.

Zodiacal light Wikipedia article. https://en.wikipedia.org/wiki/Zodiacal_light. Accessed: 2016-06-17.